http://dx.doi.org/10.5012/bkcs.2013.34.4.1296

Self-organized Artificial SEI for Improving the Cycling Ability of Silicon-based Battery Anode Materials

Jeong-Hye Min,[†,a] Young-San Bae,[‡,§,a] Joong-Yeon Kim,[‡] Sung-Soo Kim,[†] and Seung-Wan Song[†,‡,*]

[†]*Graduate School of Green Energy Technology, Chungnam National University, Daejeon 305-764, Korea*
[‡]*Department of Fine Chemical Engineering & Applied Chemistry, Chungnam National University, Daejeon 305-764, Korea*
[*]*E-mail: swsong@cnu.ac.kr*
[§]*Present affiliation: Iljin Electric Co, Ltd.*
Received January 9, 2013, Accepted January 31, 2013

Key Words : Lithium-ion battery, Anode materials, Silicon, Silicon-graphite composite, SEI layer

Silicon (Si)-based materials are considered as potential alternative anode materials to graphite for a use in the lithium-ion batteries for electric vehicles and energy storage systems because of superior theoretical capacity of 3759 $mAhg^{-1}$ at room temperature[1,2] and appropriate operation voltages of a few hundreds milivolts above lithium. However, the Si is well known to suffer from severe volume change during reaction with lithium[3] followed by electrochemical and mechanical particle disintegration[2,4] leading to a poor cycling ability. Recent reports have shown that the use of amorphous[5] or nanostructured Si,[6] and carbon-coating[7,8] or carbon composite,[9-11] and the use of advanced elastic binder[12-14] and electrolyte composition[15,16] yields enhancement of cycling ability. It still however remains a great challenge to develop new approaches for obtaining a reliable performance of lithium-ion batteries employing Si-based anodes.

Our earlier work showed that the interfacial reaction between $LiPF_6$ of commercial electrolyte and the Li_xSi deleteriously affects cycling performance.[17-20] The interfacial reaction did not provide the formation of a stable solid electrolyte interphase (SEI) layer at the Si surface but deactivates the Si gradually with cycling by surface coverage with PF-containing species together with LiF salt, while accelerating irreversible particle disintegration and a consequent and dynamic change in the active surface area. We have proposed that interfacial control is a promising approach for improving the cycling ability of Si-based anodes, which was determined based on a basic understanding of electrode-electrolyte interfacial reactions and its impacts on structural degradation and performance fade *via* electrochemical and interfacial studies of film model electrodes. Surface protection of Si was necessary both to prevent the attack by $LiPF_6$-derived species and to form a stable SEI layer.[17-20]

In the present work, we demonstrate that the cycling ability of Si nanoparticle anode is improved *via* a new approach of interfacial control. In order to suppress direct interfacial contact between Si and electrolyte while protecting the Si surface, we build up siloxane network as an artificial SEI at the surface of bulk Si active material, utilizing self-organized condensation reaction between alkoxy groups of silane molecules and hydroixde or oxygen groups of Si surface. The Si nanoparticles and composite with graphite decorated with an artificial SEI show significantly improved cycling stability.

Building up of an artificial SEI with siloxane network is simply made first by dispersing commercial Si nanoparticles in the solution of tris(2-methoxyethoxy)vinylsilane (hereafter TMVS) using ultrasonication. The presence of a trace of water in the electrolyte assists the hydrolysis and polycondensation of silanes forming the siloxane network at the Si surface. Figure 1 shows attenuated total reflection (ATR) FTIR spectral examination on the surface of Si nanoparticles before and after reacting with TMVS, together with TMVS only as a reference. For the surface of Si nanoparticles in Figure 1(c), the presence of new significant IR signatures at 1131 and 1065 cm^{-1} of Si-O-Si siloxane network,[17-19,21] compared to pristine Si nanoparticles (Figure 1(b)), confirms the formation of siloxane as an artificial SEI as illustrated in Scheme 1. Other tiny new peaks observed in Figure 1(c) provide the evidence that moiety (*e.g.*, vinyl, oxyethylene

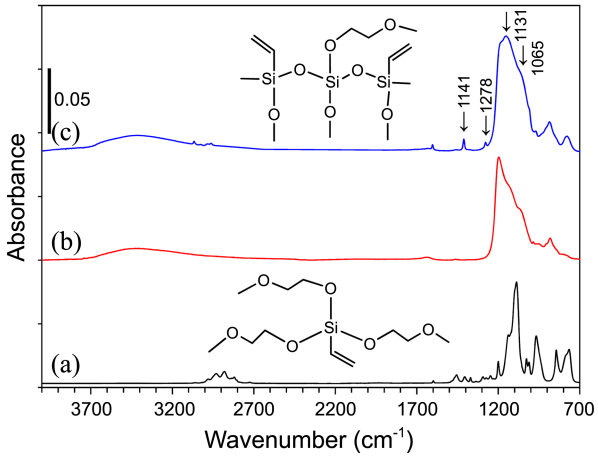

Figure 1. IR spectra for (a) tris(2-methoxyethoxy)vinylsilane (TMVS), and the surface of (b) commercial Si nanopowder and (c) Si nanopowder with self-organized siloxane surface network.

[a]These authors contributed equally to this work.

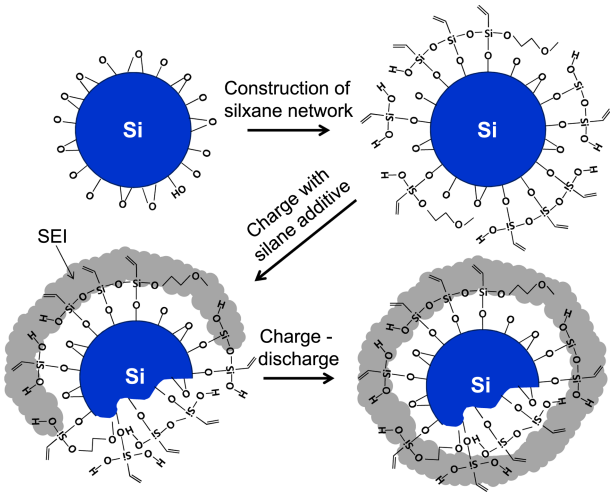

Scheme 1. Construction of an artificial SEI of siloxane surface network at the surface of silicon active material using tris(2-methoxyethoxy)vinylsilane, and compensation of damaged siloxane network upon initial charging by adding the silane as an electrolyte additive, and the SEI layer formation.

group) of TMVS, which is observed in Figure 1(a), remains as a part of an artificial SEI. Hydrophobic and organophilic vinyl and oxyethylene groups is estimated to provide the HF attack-free interface. Also vinyl group can form polymeric species by electrochemical polymerization during cycling.

In addition, a small fraction (10 wt %) of TMVS is put to the electrolyte as an additive in order to compensate a possible damage of siloxane surface network with initial charging (lithiation) and repeated cycling, as displayed in Scheme 1. In that fashion, silane molecules available in the electrolyte can play a complement role in repairing the damaged part of siloxane network due to particle cracking.

Electrochemical charge-discharge behavior of Si electrode with an artificial SEI of siloxane surface network was examined with lithium cells in 1 M $LiPF_6$/EC:EMC with 10 wt % TMVS additive between 0.1 and 1.2 V.

Figure 2(a) shows voltage profiles for five cycles of the lithium cell with Si electrode with an artificial SEI in the presence of TMVS additive. The electrode exhibits initial charge and discharge capacities of 1873 and 1296 $mAhg^{-1}$, respectively, corresponding to 69% of initial coulombic efficiency. Discharge capacity and cyclic efficiency increase after the first cycle, maintaining 1620 $mAhg^{-1}$ and 93%, respectively, to the fifth cycle. An increase in coulombic efficiency from the second cycle to 93% with well-maintained structural resolution of lithiation and delithiation in the differential capacity plots (inset) till the fifth cycle is indicative of the formation of a stable SEI layer during initial cycling. On the contrary, lower discharge capacities, lower initial coulombic efficiency (57%, 64%, respectively) and inferior cycling ability are observed when having just an artificial SEI of siloxane surface network (Figure 2(b)) or TMVS electrolyte additive (Figure 2(c)). The data indicate that early cycling ability is effectively improved when constructing and compensating the artificial SEI. Cycling-driven

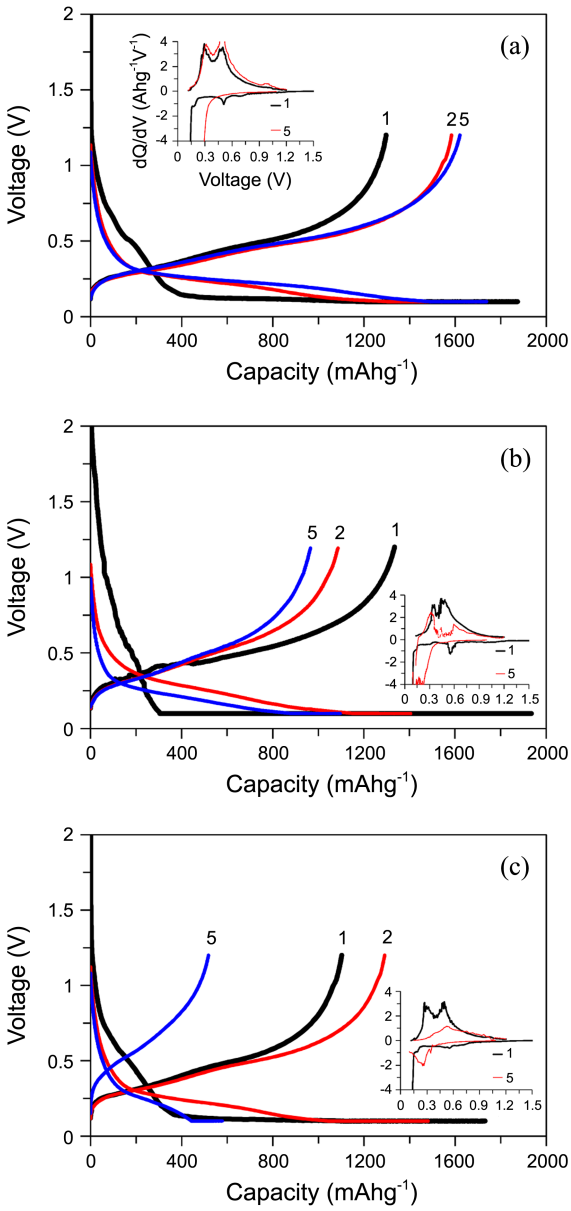

Figure 2. Voltage profiles and their differential capacity (inset) plots of the lithium cells with (a) Si electrode with an artificial SEI cycled in 1 M $LiPF_6$/EC:EMC containing 10 wt % TMVS additive, and Si electrodes only with (b) an artificial SEI or (c) with TMVS additive.

SEI formation behavior at the Si surface with an artificial SEI is investigated using *ex situ* ATR FTIR spectroscopy. In Figure 3(c) and (e), the surface of Si electrodes cycled with TMVS additive, regardless of the presence of an artificial SEI, shows in common the IR signatures of alkyl carbonate salt $ROCO_2^-M^{n+}$ (M = Li/Si), lithium carbonate Li_2CO_3, carboxylate salt $RCO_2^-M^{n+}$ and organic phosphorus fluoride (-O=PF-OR) compounds[17-26] as the SEI components, which are produced by electrolyte decomposition. However, in the absence of an artificial SEI (Figure 3(c)), a significant decrease in the peak absorbance of the SEI species is observed. Recollecting that IR absorbance is proportional to the concentration of chemical species, such remarkable

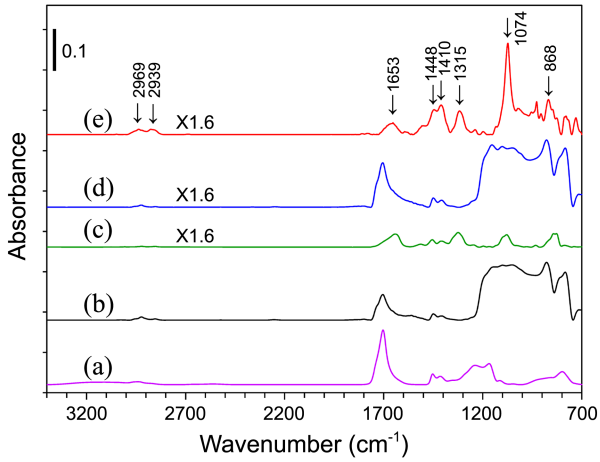

Figure 3. IR spectra for (a) polyacrylic acid binder, and the surface of (b) pristine Si electrode and (c) that after five cycles in the presence of TMVS additive, and (d) pristine Si electrode with an artificial SEI of siloxane network and (e) that after five cycles in the presence of TMVS.

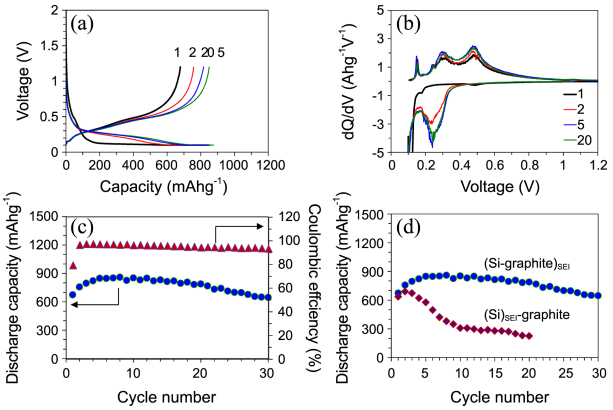

Figure 4. Voltage profiles (a), their differential capacity plots (b) and cycling ability of the lithium cells with (c) Si-graphite composite electrode with an artificial SEI, and (d) composite electrode consisting of Si with an artificial SEI and bare graphite in the presence of TMVS, as a function of cycle number.

decrease of the peak absorbance indicates a destruction or damage of the SEI layer with cycling. Siloxane surface network (Figure 3(d) and (e)) indeed plays an artificial SEI role in providing an accumulation of new SEI species with cycling. In addition, when damaged part of siloxane surface network is repaired by TMVS electrolyte additive, the Si surface enables to be effectively passivated as shown in Figure 2 and Figure 3(e). This surface protection effect induces to inhibit or reduce the mechanical caving-in event of Li_xSi particles upon simultaneous occurrence of volume change and electrolyte attack.

Interfacial stabilization *via* the construction of an artificial SEI is applied to Si-graphite composite electrode. Because of the limited cycling ability of Si electrode after five cycles, graphite is necessarily used to accommodate the volume change of Si and to promote electrical conductivity of the electrode.[27,28]

Since the vinyl group of TMVS is compatible with sp^2-hybrid carbon of graphite, it can self-organize and form an artificial SEI not only at the Si particles but also at the surface of graphite particles, as illustrated in Scheme 2. For the preparation of Si-graphite composite active materials, commercial Si nanopowders and graphite powders were mixed in the ratio of 50:50 wt % and ball-milled. Self-organization of an artificial SEI at the surface of Si-graphite composite powders was made in the same fashion to the Si.

Figure 4 shows cycling behavior of Si-graphite composite

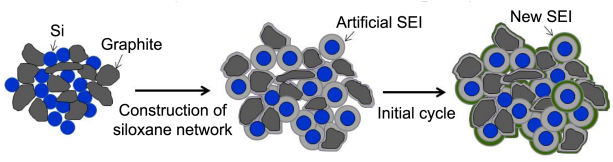

Scheme 2. Construction of an artificial SEI at the Si-graphite composite active materials and the formation of a new SEI layer during initial cycling.

electrode with an artificial SEI. The first charge and discharge capacities are 850 and 674 $mAhg^{-1}$, respectively, in Figure 4(a), where capacities are obtained from the whole weight of Si and graphite materials, resulting in the initial coulombic efficiency of 79%. The composite electrode exhibits well-maintained structural resolution due to lithiation and delithiation (Figure 4(a)-(b)) over 30 cycles, delivering discharge capacity of 859-650 $mAhg^{-1}$ with high coulombic efficiency of 94-97% and high capacity retention of 96% after 30 cycles (Figure 4(c)). In the presence of an artificial SEI at both Si and graphite composite, the electrode provides an excellent cycling ability, in contrast to a rapid capacity fade for the composite electrode consisting of Si with an artificial SEI and bare graphite, as compared in Figure 4(d). This is far better performance than that of similar bulk composite anode cycled in the presence of vinylene carbonate, which is one of the promising SEI-forming electrolyte additives.[29]

In conclusion, Si nanoparticle-based anodes with an artificial SEI of siloxane network are electrochemically tested in lithium cells. The Si anode with an artificial SEI cycled in the presence of silane electrolyte additive outperforms the ones with neither siloxane surface network nor silane electrolyte additive in terms of capacity retention and coulombic efficiency. The improved cycling ability by the presence of an artificial SEI is attributed to the surface protection effect of siloxane network, suppressing direct interfacial reaction between Si and $LiPF_6$-containing electrolyte but providing formation of a new SEI layer. Cycling ability is further stabilized by adding graphite to Si by accommodating volume change and enhancing electronic conductivity. It is believed that both the interfacial and structural stabilization is a crucial prerequisite to attain high performance lithium-ion batteries employing Si-based anodes.

Experimental

For the Si electrode fabrication, commercial Si nano-

powder (50-70 nm in diameter, 98%, Nanostructured & Amorphous Materials Inc.) was used as received. For the Si-graphite composite electrode, Si and graphite powders were mixed in the ratio of 50:50 wt % and ball-milled for 30 min. The Si powders and Si-graphite composite powders were dispersed in tris(2-methoxyethoxy)vinylsilane ((CH_2=CHSi($OCH_2CH_2)_2OCH_3)_3$, TMVS, Aldrich) by ultrasonication for 1 h at room temperature. They were then washed with anhydrous isopropanol (Aldrich) for the removal of residual silanes, followed by drying overnight in the vacuum oven at 60 °C.

The Si and Si-graphite composite electrodes were prepared by coating the slurry consisting of 80 wt % active material, 5 wt % carbon black and 15 wt % polyacrylic acid binder in *N*-methyl pyrrolidinone on a copper foil followed by drying and pressing. Lithium half-cells were assembled with Si electrode and Si-graphite composite electrode, respectively, with a surface protective layer as working electrodes and lithium counter electrode in 1 M $LiPF_6$/ethylene carbonate (EC):ethylmethyl carbonate (EMC) (3:7 volume ratio, Soulbrain) with 10 wt % TMVS additive. Electrochemical behavior of Si electrode and Si-graphite composite electrode was evaluated at the 0.033C rate in a constant current-constant voltage mode between 0.1 and 1.2 V, using a multichannel cycler (Wonatech). The 1C rate refers to the current density of 1648 mAg^{-1} applied to the cell to reach to the charge voltage of 0.1 V in 1 h. All the electrochemical experiments were conducted at room temperature in argon-filled glove box.

Surface characterization of the electrodes before and after cycling was performed using *ex situ* attenuated total reflection (ATR) FTIR spectroscopy (Thermo scientific, Nicolet 6700) using an IR spectrometer equipped with a MCT detector, without exposure to the air.

Acknowledgments. This work was financially supported by the National Research Foundation (No. 2012026203 & 2012K001255) through the MEST of Korea.

References

1. Obrovac, M. N.; Christensen, L. *Electrochem. Solid-State Lett.* **2004**, *7*, A93.
2. Weydanz, W. J.; Wohlfahrt-Mehrens, M.; Huggins, R. A. *J. Power Sources* **1999**, *81-82*, 237.
3. Bourderau, S.; Brousse, T.; Schleich, D. M. *J. Power Sources* **1999**, *81-82*, 233.
4. Kasavajjula, U.; Wang, C.; Appleby, A. J. *J. Power Sources* **2007**, *163*, 1003.
5. Ohara, S.; Suzuki, J.; Sekine, K.; Takamura, T. *J. Power Sources* **2003**, *119-121*, 591.
6. Kim, H.; Cho, J. *Nano Lett.* **2008**, *8*, 3688.
7. Dimov, N.; Kugino, S.; Yoshio, M. *Electrochim. Acta* **2003**, *48*, 1579.
8. Ng, S.-H.; Wang, J.; Wexler, D.; Konstantinov, K.; Guo, Z.-P.; Liu, H.-K. *Angew. Chem. Int. E.* **2006**, *45*, 6896.
9. Liu, Y.; Hanai, K.; Matsumura, T.; Imanishi, N.; Hirano, A.; Takeda, Y. *Electrochem. Solid-State Lett.* **2004**, *7*, A492.
10. Magasinki, A.; Dixon, P.; Hertzberg, B.; Kvit, A.; Ayala, J.; Yushin, G., *Nature Mater.* **2010**, *9*, 353.
11. Kovalenko, I.; Zdyrko, B.; Magasinski, A.; Hertzberg, B.; Milicev, Z.; Burtovyy, R.; Luzinov, I.; Yushin, G. *Science* **2011**, *75-79*, 334.
12. Lestriez, B.; Bahri, S.; Sandu, I.; Roué, L.; Guyomard, D. *Electrochem. Commun.* **2007**, *9*, 2801.
13. Magasinski, A.; Zdyrko, B.; Kovalenko, I.; Hertzberg, B.; Burtovyy, R.; Huebner, C. F.; Fuller, T. F.; Luzinov, I.; Yushin, G. *ACS Appl. Mater. Interfaces* **2010**, *2*, 3004.
14. Ryou, M.-H.; Kim, J.; Lee, I.; Kim, S.; Jeong, Y. K.; Hong, S.; Ryu, J. H.; Kim, T.-S.; Park, J.-K.; Lee, H.; Choi, J. W. *Advanced Materials* 2012.
15. Lin, Y.-M.; Klavetter, K. C.; Abel, P. R.; Davy, N. C.; Snider, J. L.; Heller, A.; Mullins, C. B. *Chem. Commun.* **2012**, *48*, 7268.
16. Dalavi, S.; Guduru, P.; Lucht, B. L. *J. Electrochem. Soc.* **2012**, *159*, A642.
17. Song, S.-W.; Baek, S.-W. *Electrochem. Solid-State Lett.* **2009**, *12*, A23.
18. Nguyen, C. C.; Song, S.-W. *Electrochim. Acta* **2010**, *55*, 3026.
19. Choi, H.; Nguyen, C. C.; Song, S.-W. *Bull. Kor. Chem. Soc.* **2010**, *31*, 2519.
20. Nguyen, C. C.; Song, S.-W. *Electrochem. Commun.* **2010**, *12*, 1593.
21. Socrates, G. *Infrared Characteristic Group Frequencies*; Tables and Charts, 2nd ed.; John Wiley & Sons: 1994.
22. Aurbach, D.; Daroux, M. L.; Faguy, P. W.; Yeager, E. *J. Electrochem. Soc.* **1987**, *134*, 1611.
23. Zhuang, G. V.; Ross, P. N. *J. Electrochem. Solid-State Lett.* **2003**, *6*, A136.
24. Daasch, L. W.; Smith, D. C. *Anal. Chem.* **1951**, *23*, 853.
25. Nyquist, R. A. *Appl. Spectrosc.* **1987**, *41*, 272.
26. Yang, H.; Zhuang, G. V.; Ross, P. N., Jr. *J. Power Sources* **2006**, *161*, 573.
27. Zhou, W.; Upreti, S.; Whittingham, M. S. *Electrochem. Commun.* **2011**, *13*, 1102.
28. Zhang, Y.; Zhang, X. G.; Zhang, H. L.; Zhao, Z. G.; Li, F.; Liu, C.; Cheng, H. M. *Electrochim. Acta* **2006**, *51*, 4994.
29. Li, M.-Q.; Qu, M.-Z.; He, X.-Y.; Yu, Z.-L. *Electrochim. Acta* **2009**, *54*, 4506.